

## Centrifuge modeling of interaction between reverse faulting and tunnel



Mohammad Hassan Baziar<sup>a,\*</sup>, Ali Nabizadeh<sup>b</sup>, Chung Jung Lee<sup>c</sup>, Wen Yi Hung<sup>d</sup>

<sup>a</sup> Center of Excellence for Fundamental Studies in Structural Engineering, School of Civil Engineering, Iran University of Science and Technology, Tehran, Iran

<sup>b</sup> School of Civil Engineering, Iran University of Science and Technology, Tehran, Iran

<sup>c</sup> Department of Civil Engineering, National Central University, Chungli, Taoyuan, Taiwan

<sup>d</sup> Department of Civil Engineering, National Central University, Chungli, Taoyuan, Taiwan

### ARTICLE INFO

#### Article history:

Received 24 July 2013

Received in revised form

12 April 2014

Accepted 26 April 2014

#### Keywords:

Centrifuge modeling

Reverse fault rupture

Tunnel

Sand

Earthquake

### ABSTRACT

In this study, a series of centrifuge tests, modeling reverse fault rupture with 60° dip angle, were conducted in a dry sandy soil with a tunnel embedded in the soil layer. The test results showed that the tunnel and soil responses depended on the tunnel position, soil relative density and tunnel rigidity. Tunnels appeared be able to deviate the fault rupture path, while this deviation may be associated with significant rotation and displacement of the tunnel. However, a deeper tunnel was able to diffuse the shear deformation to a wider zone with an unsmooth surface displacement which may cause severe damage to the surface structures. Finally, the tunnel rotation, the location of the fault outcropping, the vertical displacement of the ground surface, the effect of tunnel rigidity on fault rupture path and surface displacement and the effect of soil relative density on fault–tunnel interaction were reported and discussed in this study.

© 2014 Elsevier Ltd. All rights reserved.

### 1. Introduction

Three large magnitude earthquakes, Kocaeli and Duzce [1–7] and Chi-Chi [7–12], have revealed that fault ruptures could cause severe damages to structures especially tunnels embedded within the zone of faulting. Earthquake fault rupture might cause severe damage even to the underground structures designed to be safe against dynamic excitations. However, the earthquake engineering researchers in the past four decades have focused more on the dynamic reaction of soils and structures rather than the ground displacement due to rupture of the earth's crust.

Tunnels, being underground structures, have long been assumed to have the ability to sustain earthquake with little damage. Investigations of mountain tunnels after the Chi-Chi Earthquake in central Taiwan [10] revealed that many tunnels suffered significant damage to various extents. The results also showed that the tunnels, passing through displaced fault zone, suffered more damage by the fault throw than by the seismic loading waves.

Usually the damages induced by earthquake fault rupture can be recognized with discontinuous deformations of soil overlying

fault rupture which results in vertical or lateral offset at the ground surface.

Research on the topic of the fault rupture in free field condition and its interaction with structures can be generally categorized in the following four groups:

- (1) Case histories of surface fault rupture.
- (2) Accurate and controlled geotechnical laboratory studies, including 1-g conditions and centrifuge model tests.
- (3) Numerical modeling of fault rupture.
- (4) Analytical studies.

A series of field studies were conducted after several earthquakes in the last decade [7,9,10,13–17]. Fault movements of the 1999 Kocaeli and Duzce Earthquakes in Turkey were responsible for extensive damage to the tunnel lines [13,14]. Landslides caused by the 1930 North Izu and the 1978 Izu Oshima Island Japan earthquakes were responsible for severe damage of Tanna and Inatori Tunnels, respectively [15]. Comprehensive study of field observations from the Chi-Chi earthquake showed a marvelous interaction between the faulting phenomena and tunnel [10]. The location of tunnel appeared to be one of the most important parameters affecting the fault rupture path.

While the interaction of fault ruptures with shallow and deep foundations have been studied by a few researchers using analytical [18–21], numerical [22–30] and experimental [29,30–36] methods, very little research have been reported to investigate

\* Corresponding author. Tel.: +98 912 12515 20; fax: +98 21 77240398.

E-mail addresses: [Baziar@iust.ac.ir](mailto:Baziar@iust.ac.ir) (M.H. Baziar), [Nabizadeh@iust.ac.ir](mailto:Nabizadeh@iust.ac.ir) (A. Nabizadeh), [Cjleecciv@ncu.edu.tw](mailto:Cjleecciv@ncu.edu.tw) (C. Jung Lee), [Wyhung@ncrec.narl.org.tw](mailto:Wyhung@ncrec.narl.org.tw) (W. Yi Hung).

the behavior of tunnels located in the zone of faulting [37]. The current study presents the results of experimental studies to gain insights of the tunnels interaction with reverse fault rupture. It is hopeful, the new findings help engineers to design safer tunnels where located in the fault zone.

Unlike the surface structures such as buildings for human dwelling which occupy just a limited area, the lifeline facilities such as water supply tunnels, gas tunnels, transportation tunnels and utility tunnels, due to their extensive length, have larger probability to pass a fault rupture and therefore are very crucial to understand their interaction with rupture shear zone. In order to construct such structures close to active faults, the shape and the magnitude of fault rupture as well as the location of surface fault rupture with the presence of tunnel should be estimated, especially for the sandy soil layers. This kind of soil layers tend to develop an inclined ground surface and simultaneously scarps on the ground surface prior to reaching the shear rupture planes to the ground surface.

In this study several centrifuge tests under 80-g centrifugal acceleration have been carried out to examine the interaction of reverse fault rupture propagation in the dry sand layer with the presence of a tunnel. The effects of tunnel depth, tunnel location, soil relative density and tunnel rigidity on the fault tunnel interaction have been presented in this research. The results of these tests revealed that the location of the rupture planes in the ground can be affected by the position of tunnel and its rigidity.

Typical prototype geometry of a tunnel embedded in a dry sandy soil layer under the reverse fault rupture, studied in this research, is shown in Fig. 1. For modeling the reverse faulting, an upward displacement of the hanging wall at the bedrock was applied causing the propagation of the fault rupture through the soil layer towards the surface. With such bedrock displacement, discontinuity emerges at the ground surface and provides a boundary between the lifted hanging wall with the dip angle of 60° and the static footwall on the right side of the tunnel. The tunnel is located in the zone of faulting and hanging wall.

Based on the rupture patterns observed from the testing results, the key sketch for observation of surface rupture and distorted surface is depicted as Fig. 1. In Fig. 1,  $W$  indicates the distance from the bedrock fault to the location of the right side surface outcropping,  $\alpha$  indicates the dip angle of the fault plane,  $H$  indicates the thickness of the ground model and  $h$  indicates the vertical offset of the fault to induce the surface rupture.

## 2. Material properties

### 2.1. Soil type

Quartz sand was used for all centrifuge model tests with the unit weight of 15–16 kN/m<sup>3</sup> and the relative density of  $D_r=50$  and 70%. The tested soil is classified as poorly graded sand (SP) according to the Unified Soil Classification System (Fig. 2). The

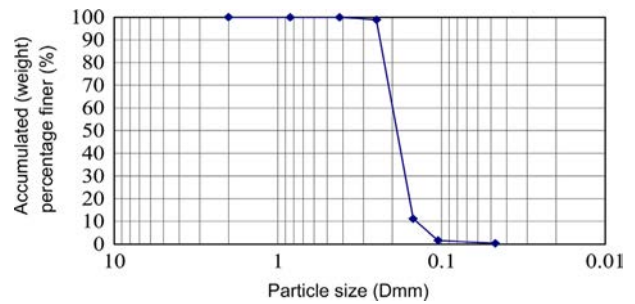


Fig. 2. Particle size distribution curve for quartz sand.

Table 1  
Physical properties of quartz sand.

Soil type	$G_s$	$\rho_{max}(g/cm^3)$	$\rho_{min}(g/cm^3)$	$d_{50}(mm)$	$d_{10}(mm)$	$\phi (D_r = 70\%)$
SP	2.65	1.66	1.38	0.193	0.147	38°

Table 2  
Mechanical properties of the aluminum alloy (6061-T6).

Unit weight (kN/m <sup>3</sup> )	Young's modulus E(GPa)	Poisson's ratio $\nu$	Tensile yield stress $f_{yk}(MPa)$	Tensile strength $f_{bk}(MPa)$
27	70	0.33	500	600

properties of crushed quartz sand were reported by Lee et al. [38]. The sand had a specific gravity ( $G_s$ ) of 2.65, and maximum and minimum dry unit weight of 16.6 kN/m<sup>3</sup> and 13.8 kN/m<sup>3</sup>, respectively with  $D_{50}=0.193$  mm and  $D_{10}=0.147$  mm. The quartz dry sand had a friction angle of 38° obtained from direct shear tests at a relative density of 70%, and a secant shear modulus  $G$  of 0.5 MPa obtained from simple shear tests at a relative density of 55% [37]. The tested sand under various stress levels had an almost linear failure envelope, with cohesion close to the zero. The dilation angle of sand was measured to be 10°–11°. Table 1 reports the properties of soil as used in this research.

### 2.2. Tunnel material type

The tunnel lining was modeled by an aluminum alloy (6061-T6) frames having an external diameter of  $D=49.4$  and 49.8 mm with a thickness of  $t=1.2$  and 1.4 mm, respectively, corresponding to  $D=4.24$  and 4.32 m with the thickness of  $t=0.24$  and 0.28 m concrete tunnel type at the prototype scale.

The tunnel thickness was selected such that the tunnel lining can resist against existed axial force and bending moment, caused by fault movement, without occurrence of large distortion or failure of lining.

The tunnels were tested using epoxy coatings with the thickness of 0.5 mm around the tunnels to model the effects of friction on the soil–tunnel interaction. The friction between the soil and the epoxy coating was about 22° according to the direct shear test for the specimen with half epoxy and half sand. The resistance of epoxy coating is much smaller than the aluminum tube and hence did not affect the rigidity of the tested tunnels.

Table 2 reports the mechanical properties of the aluminum alloy (6061-T6) used in the tests. The above properties imply that the model tube corresponds to medium flexible lining at prototype scale.

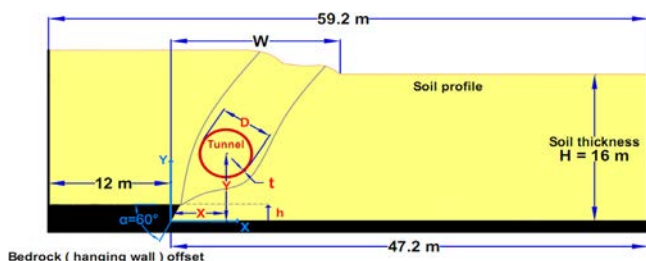


Fig. 1. Sketch of the problem and its geometry in the presented study, interaction of reverse fault rupture and tunnel.

A geotechnical centrifuge allows small-scale model testing to simulate the same physical behavior in the soil and the tunnel as in full-scale prototype tests. This is possible when the model is constructed to  $1/N$  prototype scale and is subjected to an acceleration of  $Ng$  (where  $g$  is the earth gravitation acceleration and  $N$  is the gravity level in the centrifuge test). The well-known basic scaling law for centrifuge modeling indicates:  $(EI)_{\text{model}} \times N^4 = (EI)_{\text{prototype}}$ , to ensure the similarity between the testing material and prototype material. This means the tested aluminum tube corresponds to the concrete prototype lining of the tunnel.

### 3. Centrifuge modeling and test apparatus

#### 3.1. Test procedure

All the model walls were constructed in a rectangular rigid soil container (Fig. 3), consisting of aluminum alloy frames with internal dimensions of 300 mm in width, 740 mm in length and 325 mm in height. In order to observe the faulting and shear zone of the tested models, a lucid acrylic plate window was installed at the front face of the box. The bottom of the sandbox was designed to be movable (upward and downward) and hence capable of simulating the movements of a reverse and normal faulting. The length of hanging wall was 150 mm, and the length of footwall was 59 mm. The maximum upward movement, with the  $60^\circ$  dip

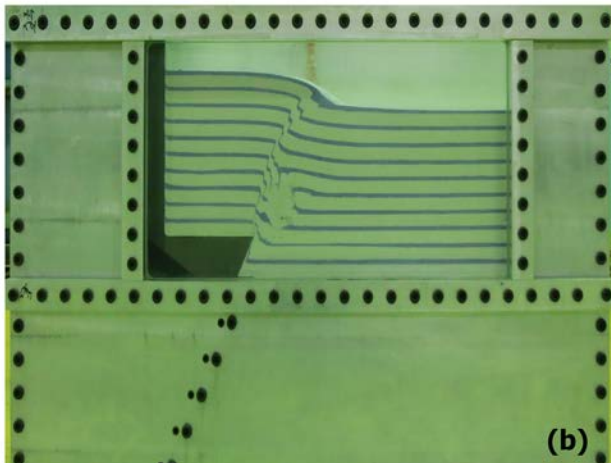
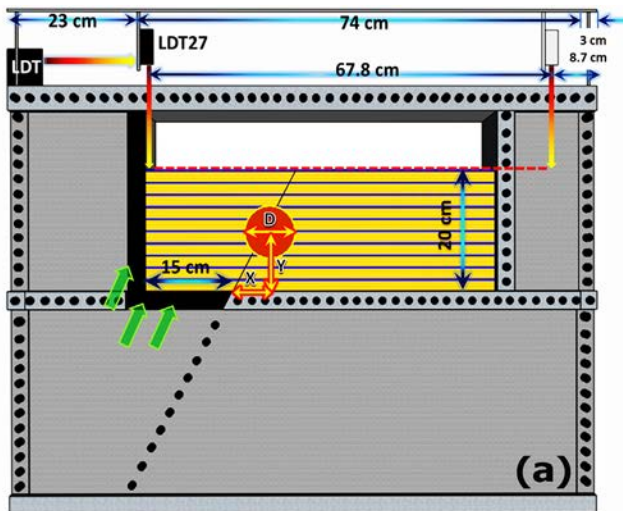


Fig. 3. The centrifuge container: (a) cross section of the experimental apparatus installed in plane strain container (dimensions in cm); (b) photograph of the apparatus (reverse fault rupture).

angle of faulting, could be as high as 50 mm. In all the tests reported here, the thickness of soil was 20 cm.

The container can simulate the normal/reverse fault slip with the speed of 0–2.5 mm/min in displacement control mode. In the laboratory, it was observed that different velocity of faulting did not have any impact on the rupture path and surface displacement in sandy soil layer. The maximum speed of faulting (2.5 mm/min) was selected to reduce the time length of performing each test.

The target centrifuge acceleration was 80-g and then faulting was carried out by moveable hanging wall. The upward movement was increased and vertical displacement of the surface was recorded at each increment of 2.5 mm of fault throw, corresponding to 0.2 m at prototype model. The upward displacement of the base was increased until the final prototype fault throw of 4 m was reached.

#### 3.2. Sample preparation

Special traveling pluviation apparatus was constructed to prepare identical and uniform relative density of the sample test in the fault box. In these experiments, layers of sand with the thickness of 1.5 cm and relative density of 50% and 70% were poured into the rigid box from the certain height and then a thin colored sand layer with the thickness of 0.5 cm were poured on each 1.5 cm layer to highlight the rupture path and shear localization from the front face. With changing the height of pouring sand and controlling the amount of pouring, the samples with different relative densities were prepared. After reaching the soil thickness to the desired value, the aluminum tube was embedded in the soil layer parallel to the fault tip. The aluminum tube was embedded at different depth and different horizontal distances ( $X$ ,  $Y$ ) from the fault tip close to the shear zone of faulting, to model the tunnel with desired position in each experiment (Fig. 3). Later, shedding the sand continued until the thickness of soil became equal to 20 cm. With measuring the weight of fault box, before and after filling the rigid box with sandy soil, the soil relative densities were obtained.

#### 3.3. Model instrumentation

At the final step of each test, the fault rupture path and shear zone were recorded by digital photography from the front face of the rigid box. A surface profile scanner, integrated with two laser displacement transducers (LDT), were installed horizontally and vertically and driven with a motor with ability of continuously scanning the elevation of the surface on the center line of the tested sand bed during the reverse faulting tests. In addition, spot measurements of vertical displacement of the soil surface were obtained using two LDT.

#### 3.4. Testing program

The centrifuge used in this study, was located in the National Central University of Taiwan (NCU), and has a nominal radius of 3 m and integrated 1D servo-hydraulically controlled shaker with a swing basket. The dimensions of the NCU centrifuge platform was 100 cm  $\times$  55 cm  $\times$  72 cm (length  $\times$  width  $\times$  height), and the maximum payload of the platform was 400 kg at an acceleration of 100 g [38,39].

A total of 7 model tests were performed in this study (Table 3). Two free-field tests with two different soil densities and soil layer depth of  $H=16$  m, and five tests with the presence of tunnel were conducted to investigate the effects of tunnel depth, tunnel location, tunnel rigidity and soil relative density on the reverse faulting tunnel interaction.

**Table 3**  
Specifications of performed centrifuge tests in this study.

Reverse fault rupture					
Test number	X (m)	Y (m)	$D_r$ (%)	Tunnel thickness (m)	Tunnel diameter (m)
1	–	–	50	–	–
2	–	–	70	–	–
3	7.36	10	70	0.24	4.24
4	5.84	8	70	0.24	4.24
5	5.84	8	50	0.24	4.24
6	4.96	6	70	0.24	4.24
7	4.96	6	70	0.28	4.32

#### 4. Test results

##### 4.1. Free field test with $D_r=50\%$

The propagation of a reverse fault rupture through dry sandy soil layer without tunnel, with  $D_r = 50\%$ , was conducted to find the pattern of fault rupture path and surface displacement in free field condition. The test result was later used to find the tunnel position in the subsequent tests such that the tunnel was in the zone of large deformation caused by faulting in all the tunnel tests.

The images, captured from the front face of the rigid box at the final stage of fault displacement, are shown in Fig. 4(b) and (c). At a final fault throw of  $h=5$  cm ( $h=4$  m in prototype scale), there is a displacement discontinuity, visible on the soil surface. An inclined zone of large shear deformation, caused by bedrock discontinuity, also occurs. The surface displacement discontinuity or localization of deformation in the left side is positioned 14.9 cm (11.9 m in prototype scale) away from the base discontinuity.

The warping and breakage of colored sand layers facilitate identification of fault rupture path, propagated into the sand layer. As the fault throw, at the base block, continues to a certain value, the fault rupture reaches to the ground surface. Small fault throws produce only a localization of deformation at the soil surface. At the final stage of fault rupture, four shear planes through the soil layer are developed. The rupture planes on the left and right sides are the major rupture planes that can reach to the ground surface and the other ruptures do not reach to the ground surface.

As the final stage of fault displacement is reached, (Fig. 4(b) and (c)), an inclined zone of large shear deformation is developed. All reverse fault rupture planes are initially propagated upward into the soil layer from the base interface almost with the same orientation as that of underlying fault plane and began to gradually decrease in dip as they approached to the soil surface. The rupture planes finally reached to the ground surface farther than the projection of fault plane with respect to the distance from the bedrock fault. Fig. 5 briefly shows the process of ground deformation at the model surface according to the different fault throws.

As seen, the soil to the right side of the fault, on the foot wall, appears relatively undisturbed, whereas the soil on the left side of the fault, on the hanging wall, has been distorted by fault propagation. The fault outcropping position on the soil surface, after the final stage of the fault throw ( $h=4$  m), is at  $X=18$  m. As seen in Fig. 5, the surface fault outcropping starts to appear (at  $X=16$  m) when the fault throw reaches to  $h=0.8$  m.

The measured surface displacement and rupture path in this study is in a very good agreement with the centrifuge test results reported by other researchers [34,35,40].

Fig. 6 shows that the surface gradient is changing in a width of ( $-2 < x < 18.5$  m) at the final fault throw,  $h=4$  m. In addition, the positions of maximum surface gradient moves away from the base

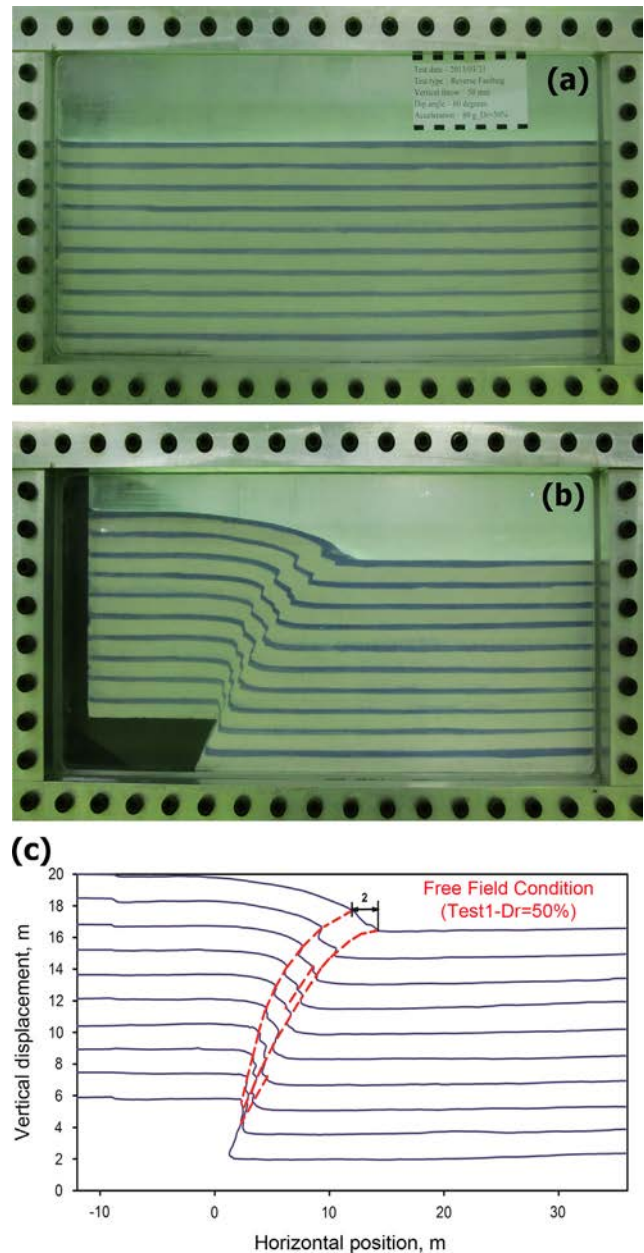


**Fig. 4.** Free-field reverse fault rupture (test 1– $D_r = 50\%$ ): Images of deformed soil specimen for fault throws (a)  $h=0$  (b)  $h=4$  m and (c) digitization on image of subsurface deformation profile at  $h=4$  m.

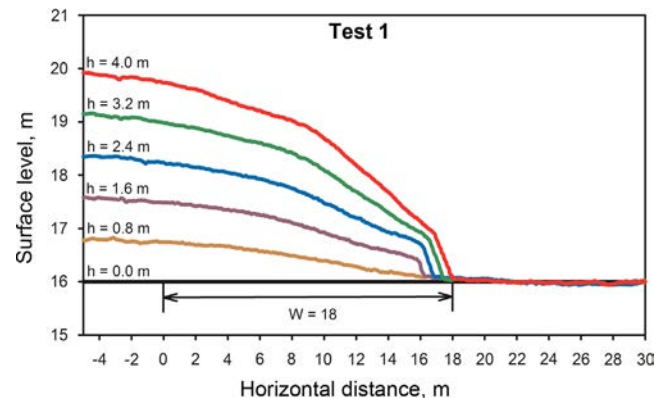


**Fig. 5.** Vertical displacements of the ground surface for the free-field condition (test 1– $D_r = 50\%$ ).

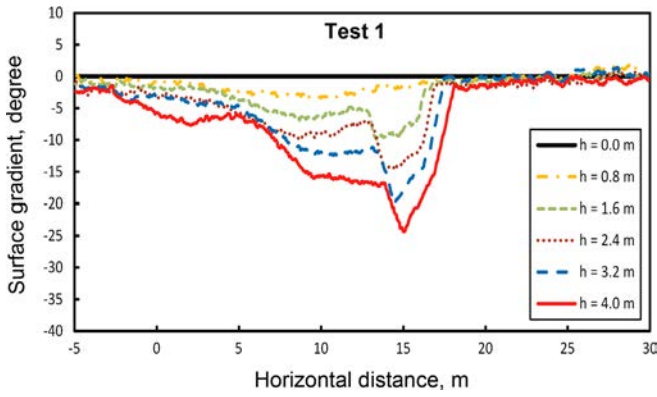


Fig. 6. Surface gradient against position for different fault throws (test 1).

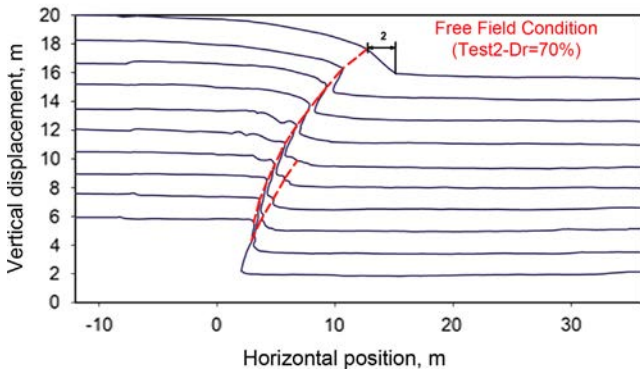
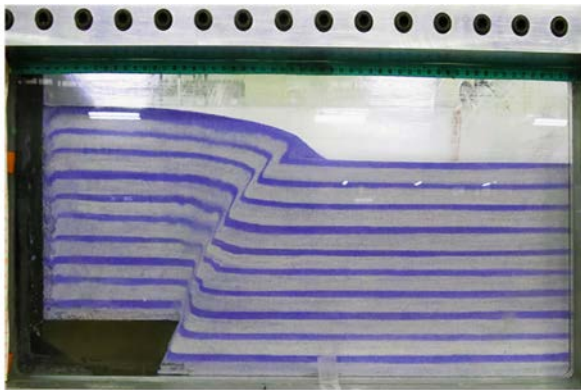


Fig. 7. Free-field reverse fault rupture (test 2— $D_r = 70\%$ ): Image of deformed soil specimen for fault throw  $h = 4$  m.

discontinuity as the fault throw increases. At  $x = 15.5$  m, where  $x$  is the horizontal distance from the fault tip, the surface gradient is the largest.

4.2. Free field test with  $D_r = 70\%$

The typical patterns of propagation of fault rupture through a dry sandy soil deposit with  $D_r = 70\%$  are illustrated in Fig. 7. As seen in this test, the left rupture reaches to the ground surface farther than the projection of fault plane compared with test 1. The fault movement in low relative density soil tends to spread out over a wider zone rather than the soil with high relative density. The shear pattern in low relative density sand is typically more complex than the high relative density models.

As the relative density of ground model became larger, the number of rupture planes appeared to be decreased. Some rupture planes, propagated into the overlying soil mass from the base, were ceased without reaching the model surface.

The surface displacement discontinuity is positioned 12.7 m away from the fault tip giving an average dip angle of  $50^\circ$  through the sand layer. The vertical component of surface displacement, measured using LDT analyses, are shown in Fig. 8. The fault outcropping position on the soil surface, after the final stage of the fault throw ( $h = 4$  m), is positioned at  $X = 17.5$  m.

Fig. 9 shows the gradient of fault rupture lines for free field tests with  $D_r = 50$  and  $70\%$ . As it is clear from this figure, the average dip angles of major ruptures are similar. These ruptures are parallel near the soil surface. The angle of fault rupture plane in the left side is steeper near the fault tip dip (fault tip dip angle =  $60^\circ$ ), but near the surface this angle is much smaller than the fault dip angle.

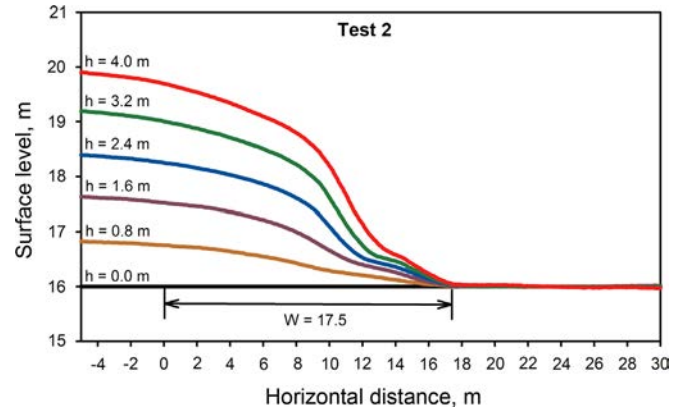


Fig. 8. Vertical displacements of the ground surface for the free-field condition (test 2— $D_r = 70\%$ ).

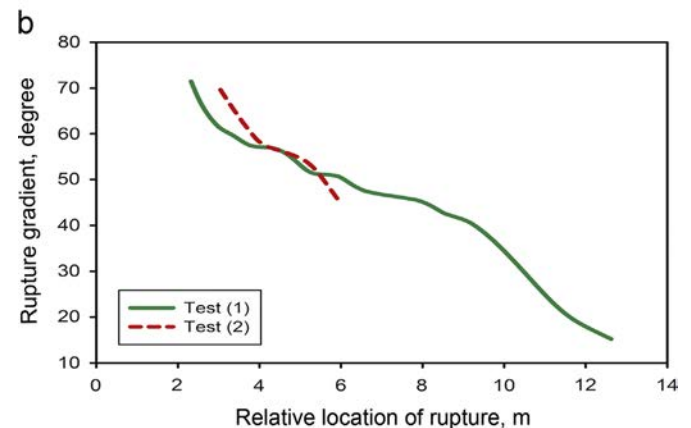
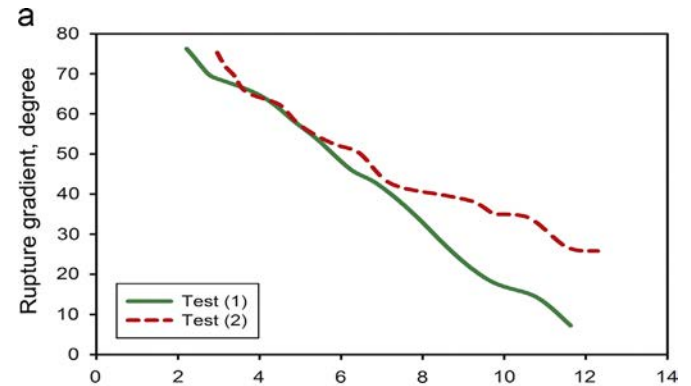


Fig. 9. Rupture gradient against position (a) right side rupture planes (b) left side rupture planes (tests 1 and 2).

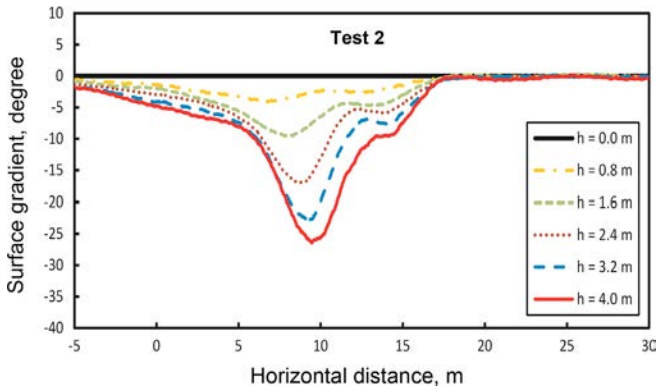


Fig. 10. Surface gradient against position for different fault throws (tests 2).

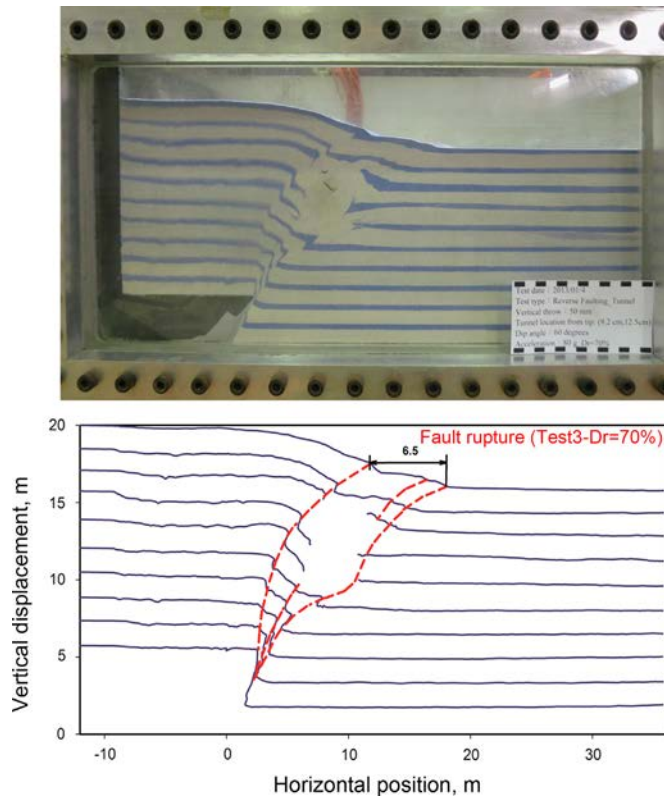


Fig. 11. Tunnel test (test 3;  $X=7.36$  m;  $Y=10$  m;  $t=0.24$  m;  $D=4.24$  m): image of deformed soil specimen for fault throw  $h=4$  m ( $D_r=70\%$ ).

Fig. 10 shows that the surface gradient is increasing over a large soil width ( $-3 \text{ m} < x < 17.5 \text{ m}$ ) toward footwall side as the fault displacement increases. The maximum surface gradient at the final stage of the test ( $h=4$  m) is about  $27^\circ$  at  $x=9.5$  m and the fault throw required for surface outcropping (at  $X=12$  m) to appear is  $h=0.8$  m.

4.3. Effect of tunnel on fault rupture path and surface displacement

In the test 3, a tunnel with diameter of  $D=4.24$  m and thickness of  $t=0.24$  m in prototype scale was embedded in the soil layer. It was positioned at ( $X=7.36$  m,  $Y=10$  m) from the fault tip which was close to the rupture path and the zone with large deformation in a free field condition.

Fig. 11 shows images captured at the final stage of test 3. From Figs. 7 and 11, the rupture paths and surface displacements, with and without tunnel, can be described. The tunnel face is visible in the soil from the front face of container. Up to 0.8 m of fault throw

(Fig. 12), no localization can be seen on the surface, while a general surface deformation of the soil in a zone of about 21 m wide on the hanging wall side can be observed. With increase of fault throw to 1.6 m (Fig. 12), localization of deformation starts to show up at the surface. As the base discontinuity increases further ( $h=4$  m), the localization moves to the right and left sides of the tunnel (Fig. 11). There are two almost parallel main rupture paths after reaching to the tunnel. The other two rupture planes, reaching the tunnel and surface, can be seen in Fig. 11.

The left rupture is deviated towards hanging wall closer to the bedrock discontinuity and the right rupture is deviated towards foot wall far away from the bedrock discontinuity. Such deviations cause an increase of average dip angle of rupture to  $56^\circ$  in the hanging wall side and a decrease of average dip angle of the rupture to  $39^\circ$  in the foot wall side. The deviation of the fault ruptures appears to protect the tunnel from significant deformation or rotation.

Therefore in test 3, the fault shear zones moved from the hanging wall side towards the footwall side and affected the area of shear zone on the ground surface to increase significantly compared with the free field condition. In summary, four fault rupture planes were developed as follow.

The first fault rupture developed from the tip of the fault to the ground surface toward hanging wall side. The second fault rupture developed from the fault tip to the ground surface toward footwall wall side and very far from the fault tip (this rupture was deviated or bent near the tunnel). The third and fourth fault ruptures began to develop toward footwall side close to the second rupture. However, one of these ruptures was ceased by the tunnel and could not reach to the surface and the other one was propagated

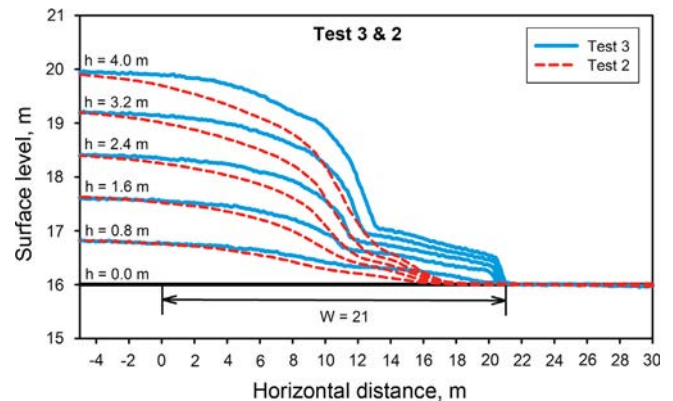


Fig. 12. Vertical displacements of the ground surface with the presence of tunnel for different fault throws (test 3– $D_r=70\%$ ).

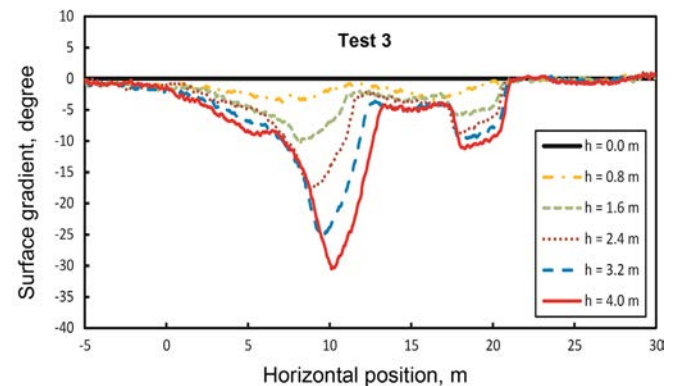


Fig. 13. Surface gradient against position with different fault throws (test 3– $D_r=70\%$ ).

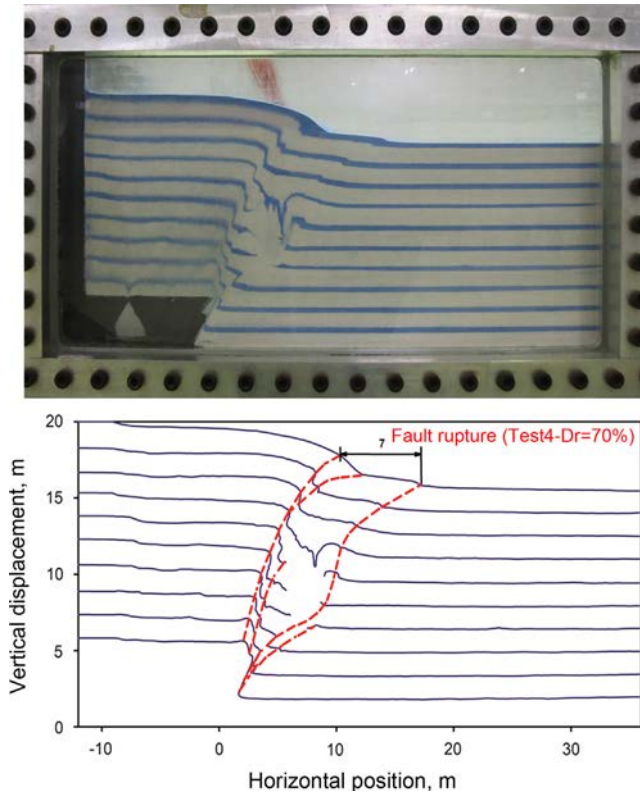


Fig. 14. Effect of tunnel position on fault tunnel interaction (test 4;  $X=5.84$  m;  $Y=8$  m;  $t=0.24$  m;  $D=4.24$  m): image of deformed soil specimen for final fault throw  $h=4$  m ( $D_r=70\%$ ).

near the soil surface. The ratio of  $W/H$  was approximately 1.31 (Fig. 12). There was a small movement or shifting of the tunnel due to the fault rupture. When compared with a site without underground tunnel, it was clearly observed that the ratio of  $W/H$  is larger due to the presence of tunnel ( $W/H$  in free field condition is 1.08) and the soil inside the zone of faulting is more severely distorted (Fig. 11).

As shown in Fig. 12, the surface displacement and surface gradient of the site with tunnel is very different with the free field condition. The surface gradient change over a large soil width ( $-2$  m  $< x < 21$  m) at the fault throw of  $h=4$  m. The maximum surface gradient at the final stage of the test ( $h=4$  m) is about  $30^\circ$  near the foot wall side and the surface gradient is the largest at  $x=10.5$  m. The location of the largest gradient is very different for the free field (Fig. 10) and with tunnel (Fig. 13).

As can be seen from Fig. 12, the surface displacement for a site with underground tunnel is unsmooth and dangerous for surface structures. In other words, the presence of shallow tunnel near the shear zone of reverse fault can result in significant damage of surface structures.

#### 4.4. Effect of burial depth on fault–tunnel interaction

As shown in Figs. 11, 14 and 15 (tests 3, 4 and 6), depth of tunnel placement has a remarkable impact on the surface fault rupture and rupture path. As the location of tunnel becomes deeper or the height of soil on top of the tunnel increases, the width of soil surface displacement increases. This might be due to the proximity of the tunnel to the fault tip which causes the rupture to deviate near the tunnel and propagate in a bigger area of soil layer. In other words, as the height of soil placed on the

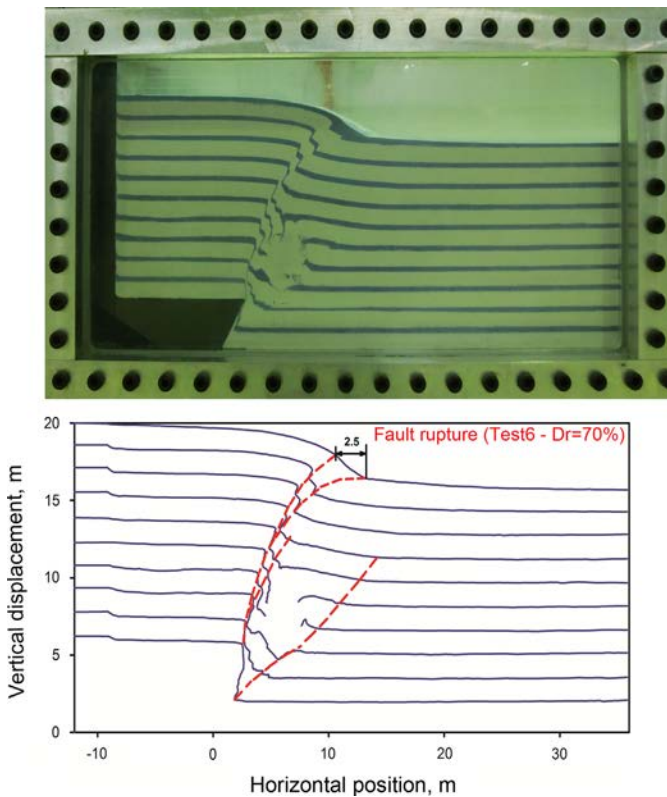


Fig. 15. Effect of tunnel position on fault tunnel interaction (test 6;  $X=4.96$  m;  $Y=6$  m;  $t=0.24$  m;  $D=4.24$  m): image of deformed soil specimen for final fault throw  $h=4$  m ( $D_r=70\%$ ).

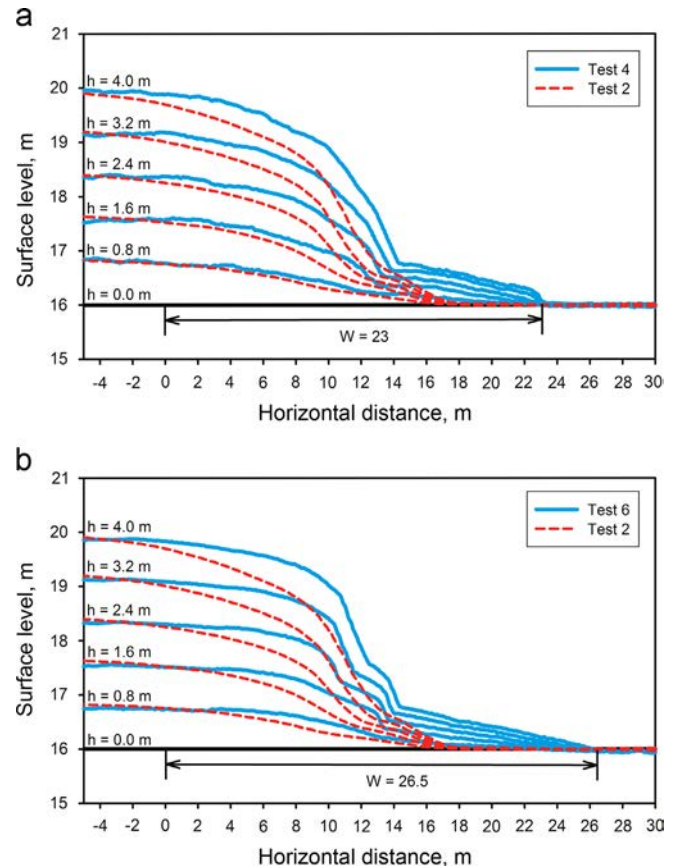


Fig. 16. Effect of tunnel position on surface displacement (a) test 4;  $X=5.84$  m;  $Y=8$  m;  $t=0.24$  m;  $D=4.24$  m (b) test 6;  $X=4.96$  m;  $Y=6$  m;  $t=0.24$  m;  $D=4.24$ .

tunnel increases, the ruptures propagate in a wider zone toward the hanging wall or footwall due to the presence of tunnel near the fault tip. As measured at the final stage of the tests 3, 4 and 6, the tunnel movement decreases with increasing the burial depth of the tunnel which was embedded close to the faulting zone.

In test 4 ( $X=5.84$  m,  $Y=8$  m) and as seen in Fig. 14 where the tunnel is close to the fault tip, the zone of large deformation develops and two main rupture planes reach to the surface. The main rupture plane near the hanging wall side is divided to two rupture planes near the soil surface. The two other rupture planes close to the fault tip cannot reach to the surface due to the presence of tunnel.

The results of test 6, the tunnel much closer to the fault tip, are shown in Fig. 15. As the ground uplift increases during faulting, faulting zone develops in an upward direction. The first fault rupture (left rupture) develops from the tip of the fault to the ground surface toward the hanging wall side, but near the fault tip

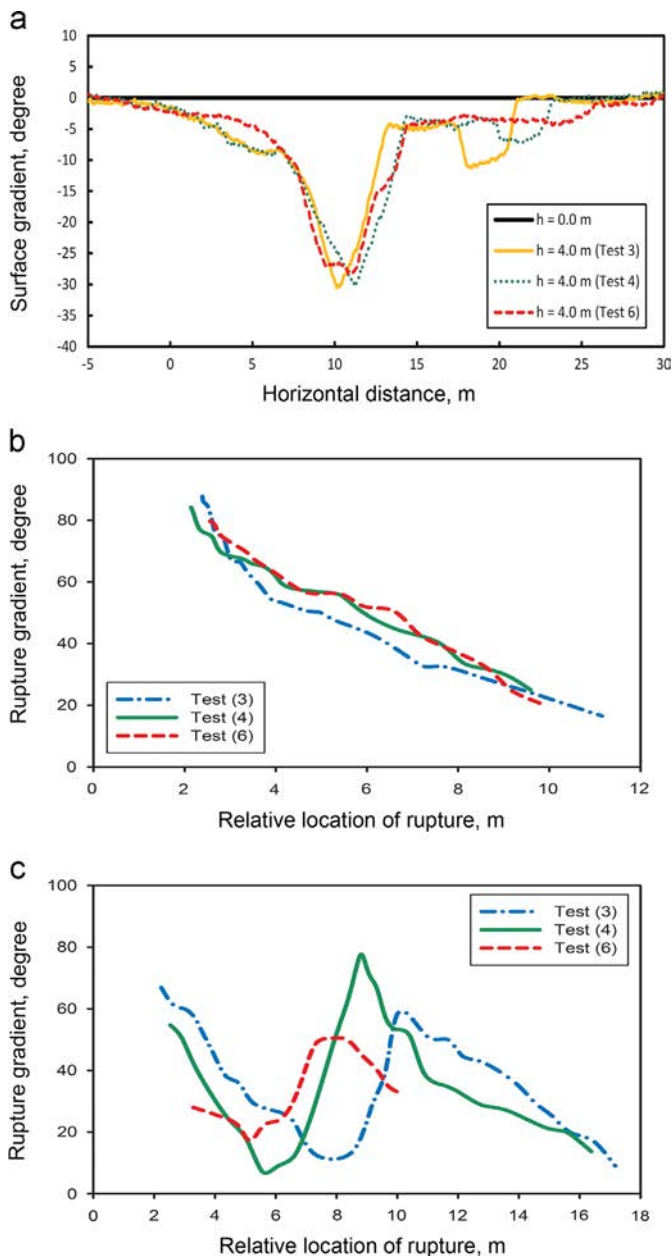


Fig. 17. Surface and rupture gradients against position for final fault throw  $h=4$  m (tests 3, 4 and 6— $D_r = 70\%$ ).

and near the soil surface this rupture plane is divided to two branches which do not completely propagate in the soil layer. The second fault rupture (right rupture) is bent by the underground tunnel and then passes near the tunnel and do not reach to the surface because of the tunnel position. Ground surface measurements indicate that the ratio of  $W/H$  is approximately equal to 1.66 (Fig. 15). After dismantling the experiment, it was found that the tunnel was moved, rotated and severely distorted. The ratio of  $W/H$  on the ground surface is much larger, compared with the case without underground tunnel or shallow tunnel. However, three distinct scarps are developed on the ground at the final fault throw ( $h=4$  m).

These tests (Figs. 11, 14 and 15) show that increasing the tunnel depth causes the tunnel and the soil layer to show more resistance against soil sliding when faulting occurs (rupture in the right side of tunnel do not reach to the ground surface due to the presence of deep tunnel).

Measurements also showed that when the tunnel is located at  $X=5.84$  m,  $Y=8$  m in test 6, there was shifting of tunnel after ground rupture with a 1.3 m vertical displacement. Where the tunnel was located at  $X=7.36$  m,  $Y=10$  m in test 3, the tunnel was distinctly shifted upward with a 1.9 m vertical displacement.

The surface displacement at different fault throws for tests 4 and 6 are shown in Fig. 16. The point of maximum surface displacement and maximum surface gradient change toward the hanging wall with increasing soil overburden pressure. In test 4 (Fig. 17(a)), the surface gradient changes in a width of  $-2 < x < 24$  m at the final fault throw ( $h=4$  m), but in test 6 the surface gradient changes in a width of  $-2 < x < 26.5$  m (Fig. 17(a)). The maximum surface gradient at the final stage of the tests ( $h=4$  m) decreases with increasing the burial depth and its location changes toward the foot wall. As can be seen in Fig. 17(b) and (c), changing the rupture gradients from the

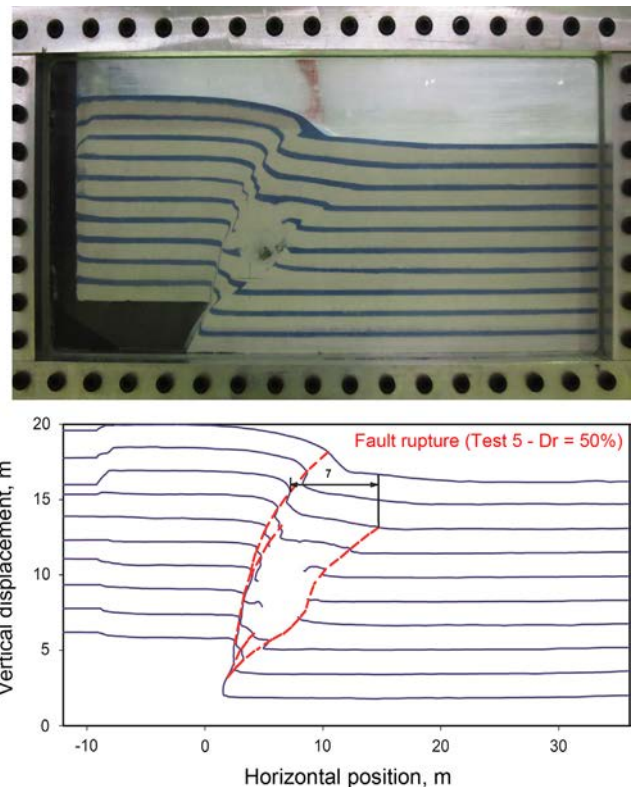


Fig. 18. Effect of soil relative density on fault tunnel interaction (test 5;  $X=5.84$  m;  $Y=8$  m;  $t=0.24$  m;  $D=4.24$  m); image of deformed soil specimen for final fault throw  $h=4$  m ( $D_r = 50\%$ ).

bedrock discontinuity to the ground surface in the tests 3, 4 and 6 are similar.

4.5. Effect of soil relative density ( $D_r$ ) on fault–tunnel interaction

To study the effect of soil relative density on the fault tunnel interaction, two tests of 4 and 5 were conducted. As indicated in Figs. 14 and 18, in test 4 ( $D_r = 70\%$ ) with the presence of tunnel, the main rupture on the right side of tunnel reaches to the ground surface, but in test 5 ( $D_r = 50\%$ ), the rupture on the right side of the tunnel does not reach to the ground surface. Particularly for the soil with higher relative density, the number of developed shear planes is larger. In addition, the presence of tunnel causes the fault plane reach to the ground surface such that to create zone of large deformation with  $W=24$  m (Figs. 14 and 18).

On the other hand, with the presence of tunnel, the change in soil relative density showed different trend regarding the pattern of developing shear planes. As shown in Fig. 18, the model with  $D_r = 50\%$  generates two continuous rupture planes. The left side rupture reaches to the surface; but the right side rupture does not reach to the soil surface. Therefore in soft soil, the tunnel attracts the faulting pressure in early stages of the fault throw. After compressing the soil between the fault tip and the tunnel, the rupture starts propagating in the soil layer. This appeared with increasing the fault throw up to 4 m ( $h > 4$  m) and the main rupture in right side reached to the surface. At the final stage of the fault throw ( $h=4$  m), the number of rupture planes in the model with 50% relative density is less than the model with 70% relative density. In addition, it seems the shear pattern in soil layer with high relative density is typically more

complex than in lower relative density models due to the presence of tunnel.

As seen in Fig. 18, the first fault rupture developed from the tip of the fault to the ground surface toward hanging wall side. However this rupture, near the fault tip and the soil surface, was divided to two branches and then these branches could not completely propagate in the soil layer; the second fault rupture was bent by the underground tunnel, passing near the tunnel, and did not reach to the ground surface. Ground surface measurement indicated that the value of  $W/H$  on the ground surface is approximately equal to 1.51 (Fig. 19(a)).

Fig. 20 indicates that the surface localization in the right side of shear zone is positioned 13.8 m away from the fault tip giving an average dip angle of  $38^\circ$  through the sand layer. This angle is similar to the case with 70% soil relative density (test 4). The vertical components of surface deformations, measured by LDT analyses, are shown in Fig. 19(a). Five distinct scarps can be seen on the surface at the final fault throw ( $h=4$  m) for test 5, while three scarps were developed in test 4 at  $h=4$  m. In addition, the surface deformation in low relative density soil is more complex and unsmooth than in the model with high soil relative density.

Fig. 19(b) shows that the surface gradient is changing over a large soil width of  $-2 \text{ m} < x < 26.5 \text{ m}$  at the fault throw of  $h=4$  m, with about  $26^\circ$  largest gradient at  $x=13$  m. As a result of test 5 and Fig. 18, it can be said that the rupture path is inclined toward the foot wall side and the zone of large deformation becomes wider.

4.6. Effect of tunnel rigidity ( $EI$ ) on fault–tunnel interaction

The same conditions as the test 6 were duplicated in test 7 except that the tunnel had higher rigidity;  $D=4.32$  m and  $t=0.28$  m instead of  $D=4.24$  m and  $t=0.24$  m. Images capturing fault propagation for

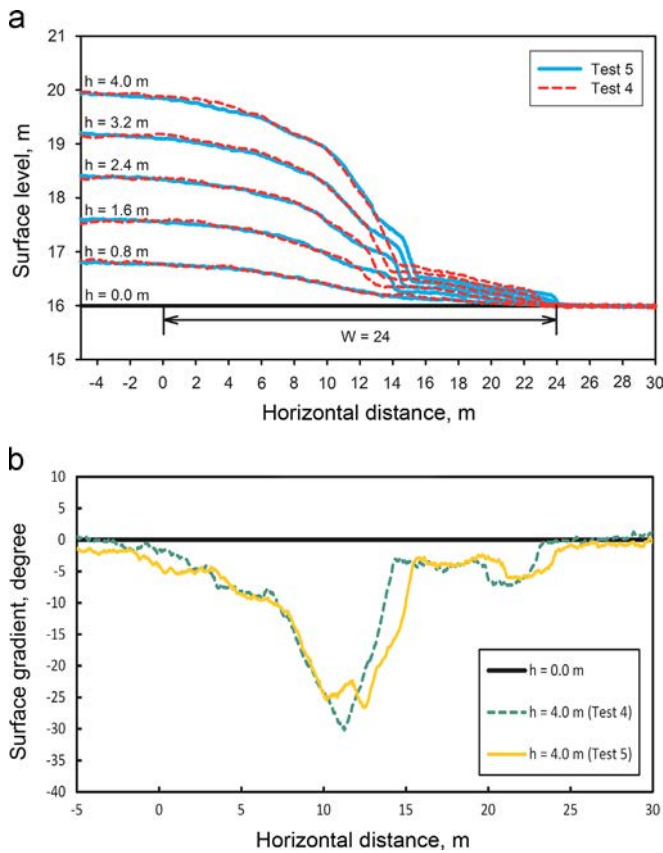


Fig. 19. Effect of soil relative density on fault tunnel interaction (tests 4 and 5;  $X=5.84$  m;  $Y=8$  m;  $t=0.24$  m;  $D=4.24$  m); (a) vertical displacements of the ground surface for different fault throws (b) surface gradients against position for final fault throw  $h=4$  m.

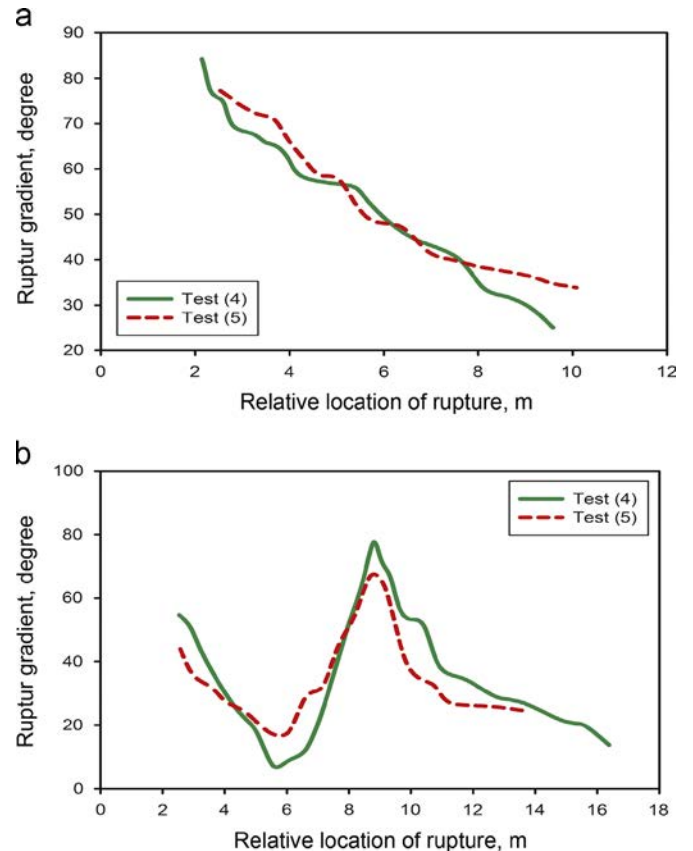


Fig. 20. Rupture gradients against position for final fault throw  $h=4$  m (a) left rupture (b) right rupture (tests 4 and 5— $D_r = 50-70\%$ ).

test 7 are shown in Fig. 21. As seen in Fig. 22(a), no localization is visible at the soil surface for a fault throw of  $h=0.8$  m and the first localization of deformation becomes visible where  $h=1.6$  m. For the final fault throw of 4 m (Fig. 21(b) and (c)), there is a clear rupture path in the left side of the tunnel toward hanging wall. However no shear localization for rupture in right side is evident near the ground surface. Therefore for tunnel with high rigidity, the right side rupture path does not reach to the ground surface and this rupture stops under the tunnel. The length of right side rupture in test 6 is longer than the length of right rupture in test 7.

The mechanism of the soil deformation for high rigidity tunnel is similar to the low rigidity tunnel except that the number of scraps on the soil surface increases for the low rigidity tunnel. The rigid tunnel can cease the rupture path and affect a small area of the soil layer. Instead, in low rigidity tunnel, the rupture path bends near the tunnel and reaches to the ground surface (there are many localization of deformation on soil surface). As measured after dismantling the

experiment, the movement of high rigidity tunnel is less than the low rigidity tunnel. The maximum surface gradient at the final stage of the test 7 ( $h=4$  m) is about  $23^\circ$  (Fig. 22(b)) at  $x=15$  m (this point is different compared with the low rigidity tunnel).

In test 7, the rupture path is inclined to the foot wall side, but the zone of large deformation is similar with test 6. The higher rigidity tunnel reduces localization of deformation in the soil surface with attracting the faulting pressure and as a result, the number of scraps on the ground surface decreases. This suggests that the tunnel with high rigidity prevent the fault localization particularly near the soil surface in the foot wall side. This observation is important for considering the interaction of the tunnels with surface structures.

### 5. Discussion

Schematic explanations of the possible fault–tunnel interaction mechanisms are presented in Fig. 23. Six possible mechanisms are predictable based on those observed in the centrifuge tests:

(a) Mechanism 1 where the fault emerges on the ground surface in loose sandy soil in free field condition Fig. 23(a). (b) Mechanism 2 where the fault emerges on the ground surface in sandy soil with medium relative density in free field condition Fig. 23(b). (c) Mechanism 3 where a shallow tunnel was embedded inside the zone of faulting Fig. 23(c). (d) Mechanism 4 where a deep tunnel was embedded inside the zone of faulting Fig. 23(d). (e) Mechanism 5 where the fault emerges on the ground surface in loose sandy soil with the presence of tunnel embedded inside the zone of faulting Fig. 23(e). (f) Mechanism 6 where the fault

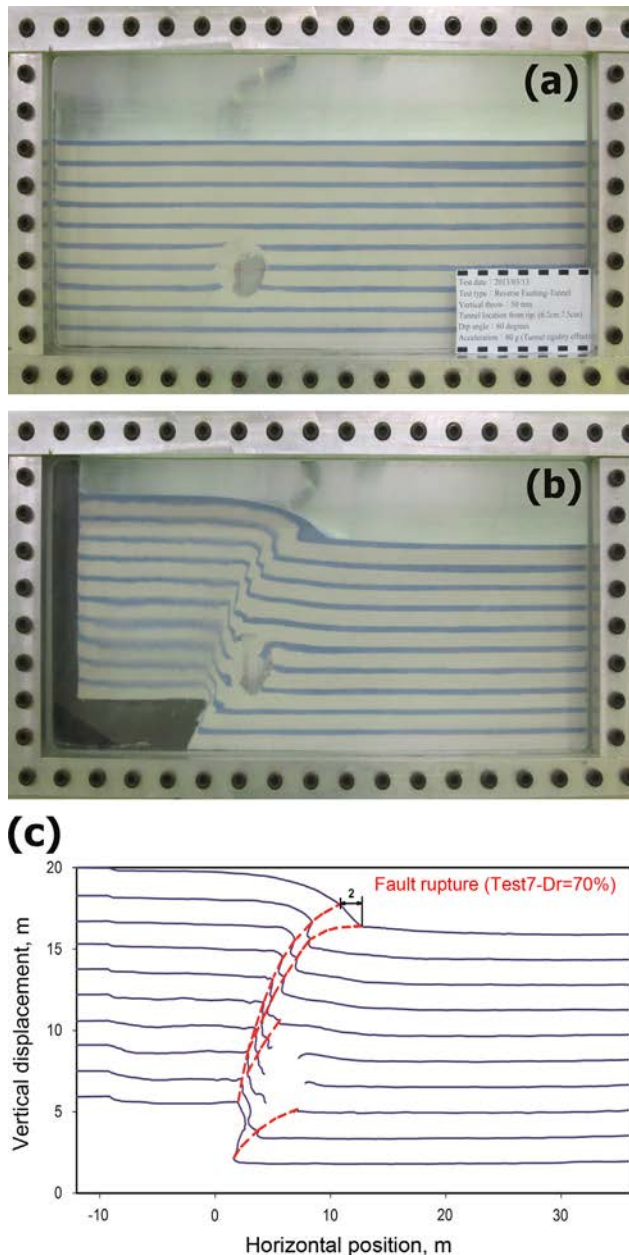


Fig. 21. Effect of tunnel rigidity on fault tunnel interaction (test 7– $D_r=70\%$ ): Images of deformed soil specimen for fault throws (a)  $h=0$  (b)  $h=4$  m and (c) digitization on image of subsurface deformation profile at  $h=4$  m.

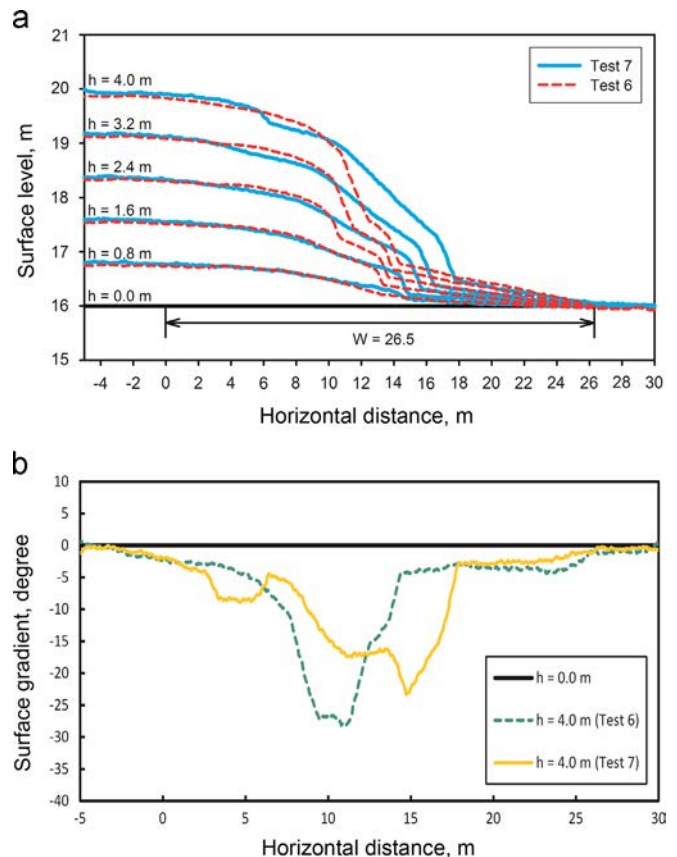
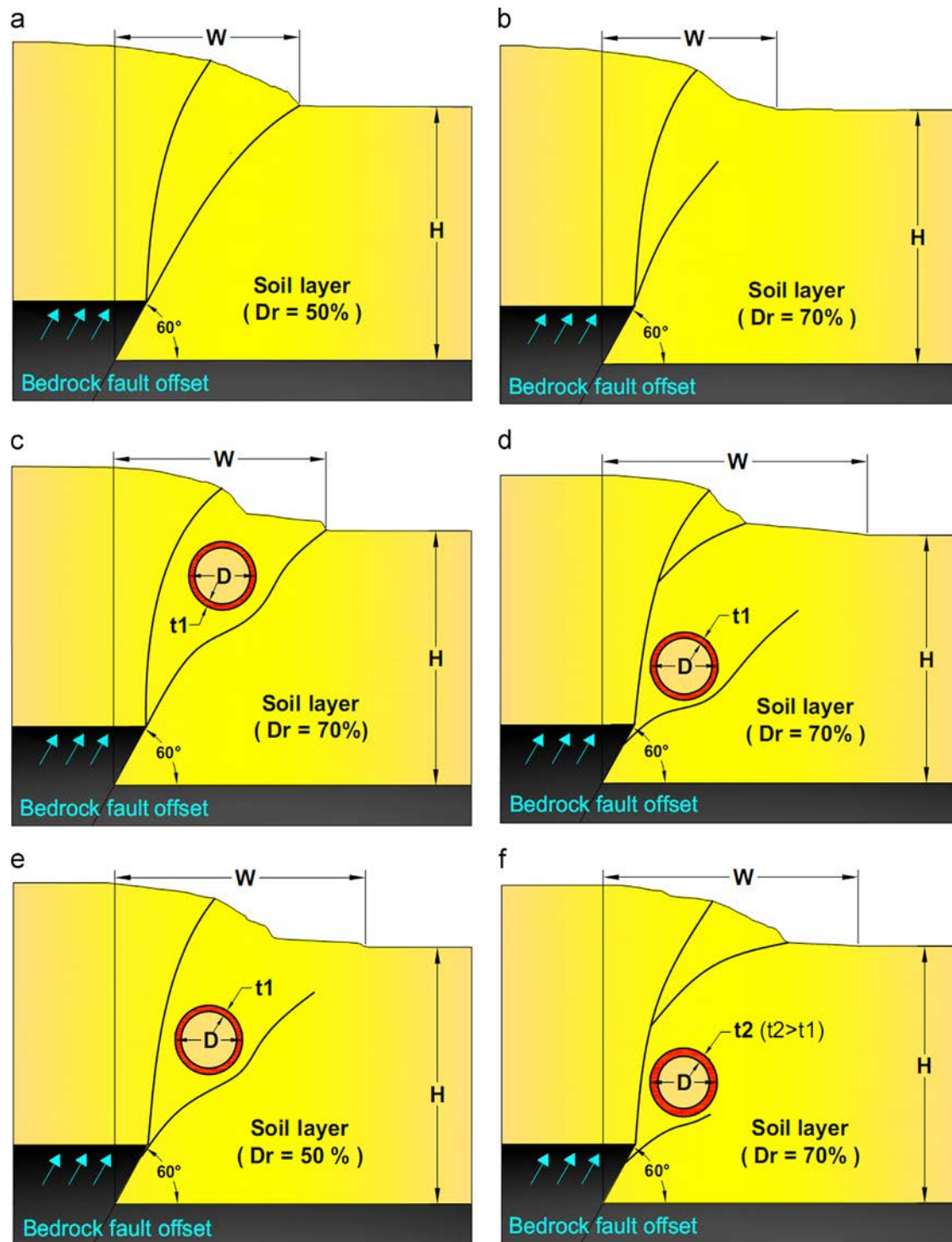


Fig. 22. Effect of tunnel rigidity on fault tunnel interaction; (tests 6 and 7) (a) Vertical displacements of the ground surface for different fault throws (b) surface gradients against position for final fault throw  $h=4$  m ( $D_r=70\%$ ).



**Fig. 23.** Fault–tunnel interaction mechanisms (a) mechanism 1: free field with  $D_r = 50\%$  (b) mechanism 2: free field with  $D_r = 70\%$  (c) mechanism 3: effect of shallow tunnel (d) mechanism 4: effect of deep tunnel (e) mechanism 5: effect of soil relative density (f) mechanism 6: effect of tunnel rigidity.

emerges on the ground surface with the presence of high rigidity tunnel embedded inside the zone of faulting Fig. 23(f).

The mechanisms 1 and 2 are similar with the centrifuge test results reported by Lee and Hamada [40], Bransby et al. [34] and Ahmed and Bransby [35].

Mechanism 3, Fig. 23(c), where the tunnel is located close to the ground surface, two fault rupture path develops and reaches to the ground surface. When these ruptures encounter the tunnel, they are hampered and bent by the underground tunnel, and then pass close to the tunnel. The other concentrated ruptures develop

upward toward the hanging wall or the foot wall; these ruptures do not propagate in a total soil layer, but increase the scraps on the ground surface. The zone of large soil deformation at the ground surface is developed which affects a large area of the ground surface. In test 2 (free field condition) the width of zone with large soil deformation is much smaller than the test 3 or test 4. These two phenomena are very dangerous for surface structures and should be considered in the design of surface structures. The position of maximum surface gradient and surface displacement are changed due to the presence of tunnel. In addition, it was

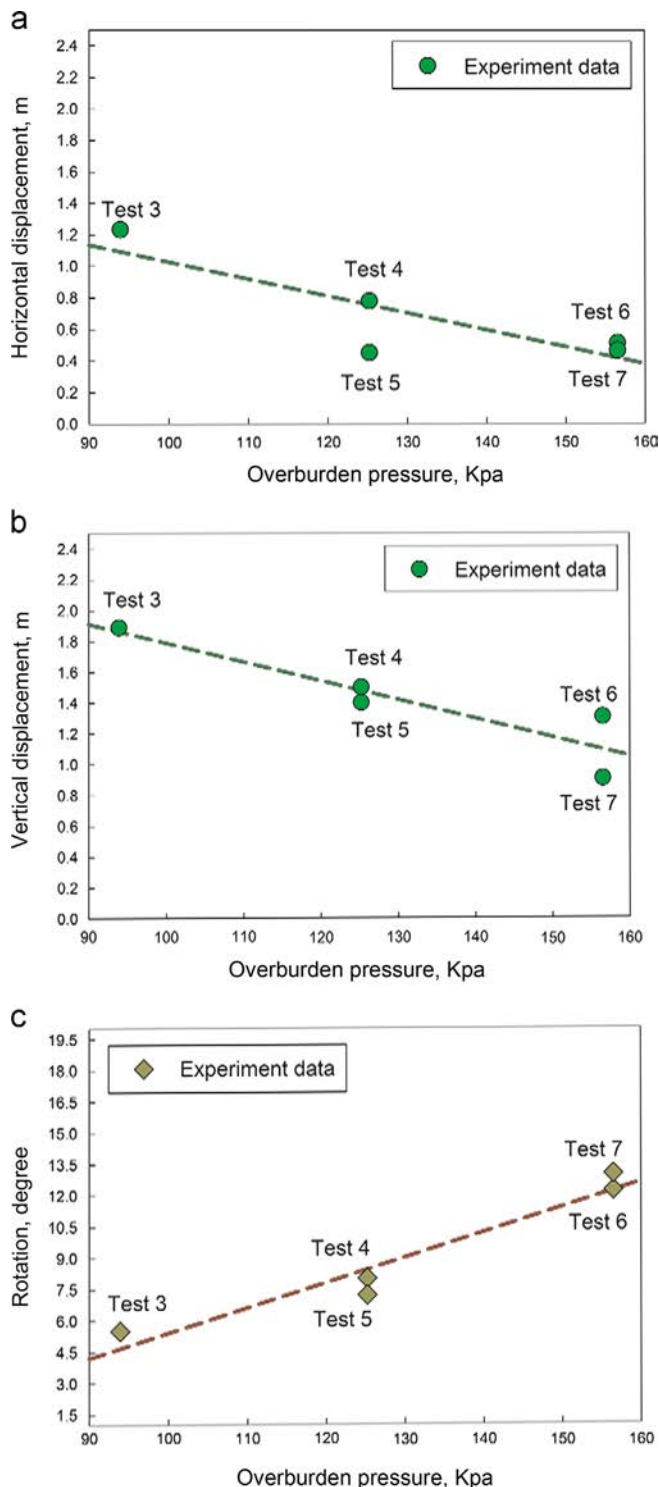


Fig. 24. Tunnel movement against overburden pressure for the final fault throw;  $h=4$  m (a) horizontal movement of the tunnel (b) vertical movement of the tunnel (c) tunnel rotation.

observed that the tunnel was deformed and rotated due to fault rupture.

Mechanism 4, Fig. 23(d), shows that the presence of a deep tunnel affects the displacement and the deformation of the ground as well as the development of the faulting zone within the soil layer. Therefore with increasing the depth of tunnel, the faulting zone develops toward the foot wall and affects the greater surface area. Also the number of scraps on the surface increases with increasing the tunnel depth. The right side rupture path for the

deep tunnel does not reach to the surface (the deep tunnel attracts the faulting pressure). When the tunnel is located in the zone of faulting and very close to the fault tip, it was observed that the rotation and deformation of the tunnel is relatively significant. Meanwhile, the development of the fault ruptures and the zone of faulting are affected by the presence of tunnel and tunnel depth. The tunnel is also significantly deformed and the development of the zone of large deformation is completely affected by the tunnel.

However, the tunnel is substantially displaced according to the slide direction of the underlying bedrock. When the tunnel is located outside the faulting zone, recognized in free field condition, the faulting does not have an interaction with the existence of tunnel. In this condition, the rupture path and the surface displacement is similar to the free field fault rupture.

Mechanism 5 describes the embedded tunnel in loose sandy soil and inside the faulting zone. The left fault rupture emerges on the hanging wall side and the right side rupture does not reach to the surface. The number of scraps on the ground surface increases for loose sandy soils which is very important for designing the surface structures.

For a stiffer soil, the development of the fault zone tends to be wider and inclined toward the footwall and it is enlarged due to the decrease of soil relative density. However, the increase of soil relative density does not seem to affect the displacement and the deformation of the tunnel.

Fig. 23(f) shows mechanism 6 where the high rigid tunnel was positioned close to the fault tip, thus preventing mechanism 4. Due to the presence of rigid tunnel, the rupture path does not propagate in the right side of the tunnel. The zone of large deformation on the ground surface is similar to the low rigid tunnel. As seen in Fig. 22(a), the number of scraps and the localization of deformations on the ground surface decrease due to the presence of rigid tunnel. Based on the observed deformed shape of the tunnel after dismantling the specimen, it was concluded that the axial force and bending moment in the lining around the tunnel was decreased. It can be said that this mechanism is similar to the case with low rigid tunnel, but with larger surface fault displacement where again; the kinematics of the shear planes can be bent to pass from the tunnel in the right side and reach up to the surface.

Considering the above mechanisms, it appears that when the tunnel was near the fault tip, the faulting pressure was propagated in the small area of the sandy soil layer before reaching to the tunnel. Therefore higher faulting pressure reached to the tunnel. It was concluded that the required strength of the tunnel for diverting the rupture path for this tunnel condition was higher. When the tunnel was far from the fault tip, the faulting pressure was propagated in the larger area and the required strength of the tunnel for diverting the rupture path was smaller. Thus, the soil behaves like mechanism 3 in the case of shallow tunnel and like mechanism 4 for the deep tunnel. In the other words, the fault rupture planes select the path based on the position of the tunnel relative to the fault tip, the depth of the tunnel, tunnel rigidity and soil relative density. The above results show that there is a significant interaction between reverse fault rupture planes and tunnels. In these cases due to the presence of tunnel inside the faulting zone, the fault rupture path is able to deflect away compared with free field condition. Therefore, it is possible to design tunnels or surface structures, taking into account fault rupture–soil–tunnel interaction. However, while the tunnel position, its depth and rigidity appear critical for the design process, knowing precisely the fault rupture path is still a difficult task.

For a deeper tunnel, the fault rupture may be stopped beneath the tunnel (Fig. 23(f)). For this case, the tunnel experiences significant rotation as well as large bending moments and axial forces. Therefore it is suggested that deep tunnels near the faulting

**Table 4**Characteristics of ruptures with and without the presence of tunnel after the final fault throw ( $h=4$  m).

Test condition	Test number	W (m)	Number of ruptures	Number of scraps	Maximum surface gradient (degree)	Affected width on the soil surface (m)
Free field ( $D_r = 50\%$ )	1	18	4	2	24	20.5
Free field ( $D_r = 70\%$ )	2	17.5	2	2	27	20.5
Effect of shallow tunnel	3	21	4	3	30	23
Effect of deep tunnel	6	26.5	4	4	28	28.5
Effect of soil density	5	24	4	5	26	28.5
Effect of tunnel rigidity	7	26.5	4	3	23	29.5

path should be rigid and an increase in their rigidity may be useful for their performance.

Fig. 24 shows the values of rotations, vertical and horizontal movements of the tunnel for different burial depth. As seen, with increasing the burial depth of tunnel, the vertical and the horizontal displacements of the tunnel decrease and the tunnel rotation increases. With increasing the tunnel rigidity, the values of tunnel rotation and horizontal displacement for both rigidities are similar, but the vertical displacement decreases with increasing the tunnel rigidity.

In tests 3, 4 and 5 the tunnel linings did not show any damage, while in tests 6 and 7 the tunnel linings were deformed and damaged. In tests 3, 4 and 5, the tunnels were only displaced and rotated without showing any deformed shape.

Also, Table 4 compares the characteristics of ruptures with and without the presence of tunnel after the final fault throw ( $h=4$  m). The value of  $W$ , the affected width on the ground surface and the number of ruptures increase due to the presence of tunnel.

## 6. Conclusions

A comprehensive centrifuge study on the fault rupture–soil–tunnel interaction in earthquake reverse faulting was reported and discussed in this research. The research focused on the investigation of the influence of important factors such as: tunnel position, tunnel depth, tunnel rigidity and soil relative density on the reverse fault tunnel interaction. As a consequence of such interaction: fault rupture path, surface displacement, surface gradient, rupture gradient and shear zone position were reported in this study. Based on the results of this research, the following conclusions can be drawn:

- (1) The burial depth of tunnel influences the zone of faulting and the relevant rupture path or shear plane in dry sandy soils. The centrifuge modeling suggests that for shallow and medium burial depth of tunnel, failure mechanism 3, two main fault rupture path can reach to the surface. The zone of large deformation was larger than the free field condition. For deep burial depth, failure mechanism 4, only one rupture plane can reach to the ground surface. The zone of large deformation, in this case develops in an area larger than the shallow depth tunnels. Therefore with increasing the burial depth of tunnel, the zone with large deformation becomes wider. It can be concluded that the soil pressure, induced by reverse faulting, on the tunnel lining increases with increasing the burial depth.
- (2) The tunnel rigidity can be influential in determining the fault rupture path. Whenever the rigidity increases, the tunnel tends to attract the faulting pressure and causes the change in the direction of faulting.
- (3) Many factors affect the tunnel rotation and movement in the faulting–tunnel interaction including: (a) The position of tunnel relative to the fault tip (b) the amount of tunnel

rigidity. For the values modeled in the present study, when the tunnel was close to the fault tip, the tunnel rotation reached to its maximum and its movement reached to its minimum. If the tunnel is located in the footwall or far enough from the free field fault rupture, it is not threatened by reverse fault rupture.

- (4) When the tunnel is embedded in a soil layer, the number of scraps and the amount of differential displacement (slope) at the surface are increased. This increase of differential displacement is highlighted with more increase in the fault displacement.
- (5) With the presence of tunnel, as the relative density of soil become greater, the number of rupture planes decreases. Some rupture planes, propagated into the overlying soil mass from the base, are ceased without reaching the surface. In addition, the tunnel in reverse fault condition causes the fault movement to propagate to the ground surface spreading out over a wider faulting zone rather than the similar case with higher relative density soil layer.
- (6) For shallow tunnel and having enough distance to the fault tip, the rigidity of tunnels can be reduced.

## References

- [1] Youd TL, Bardet JP, Bray JD. Kocaeli-Turkey earthquake of August 17 1999, reconnaissance report. *Earthquake Spectra* 2000;16(Suppl A).
- [2] Bray JD. Developing mitigation measures for the hazards associated with earthquake surface fault rupture. In: Proc. workshop on seismic fault-induced failures—possible remedies for damage to urban facilities, Japan: University of Tokyo; 2001. p. 55–79.
- [3] Ulusay R, Aydan Ö, Hamada M. The behavior of structures built on active fault zones: examples from the recent earthquakes in Turkey. In: Seismic fault-induced failures—possible remedies for damage to urban facilities. Japan: University of Tokyo; 2001. p. 1–26.
- [4] Pamuk A, Kalkanb E, Linga HI. Structural and geotechnical impacts of surface rupture on highway structures during recent earthquakes in Turkey. *Soil Dyn Earthquake Eng* 2005;25:581–9.
- [5] Anastasopoulos I, Gazetas G. Foundation–structure systems over a rupturing normal fault: Part I. Observations after the Kocaeli 1999 earthquake. *Bull Earthquake Eng* 2007;5(3):253–75.
- [6] Anastasopoulos I, Gazetas G. Behaviour of structure–foundation systems over a rupturing normal fault: Part II. Analysis of the Kocaeli case histories. *Bull Earthquake Eng* 2007;5(3):277–301.
- [7] Faccioli E, Anastasopoulos I, Gazetas G, Callerio A, Paolucci R. Fault rupture–foundation interaction: selected case histories. *Bull Earthquake Eng* 2008;6(4):557–83.
- [8] Chen CC, Huang CT, Cherng RH, Jeng V. Preliminary investigation of damage to near fault buildings of the 1999 Chi-Chi earthquake. *Earthquake Eng Eng Seismol* 2000;2(1):79–92.
- [9] Kelson KI, Kang KH, Page WD, Lee CT, Cluff LS. Representative styles of deformation along the Chelungpu fault from the 1999 Chi-Chi (Taiwan) earthquake: geomorphic characteristics and responses of man-made structures. *Bull Seismol Soc Am* 2001;91(5):930–52.
- [10] Wang WL, Wang TT, Su JJ, Lin CH, Seng CR, Huang TH. Assessment of damages in mountain tunnels due to the Taiwan Chi-Chi Earthquake. *Tunnelling Underground Space Technol* 2001;16:133–50.
- [11] Yang HW, Beeson J. The setback distance concept and 1999 Chi-Chi (Taiwan) earthquake. In: Prakash S, editor. Proceedings of the fourth international conference on recent advances in geotechnical earthquake engineering and soil dynamics. CD-ROM, paper no. 10.56. San Diego: California, University of Missouri-Rolla; 2001.

- [12] Dong JJ, Wang CD, Lee CT, Liao JJ, Pan YW. The influence of surface ruptures on building damage in the 1999 Chi-Chi earthquake: a case study in Fengyuan City. *Eng Geol* 2004;71(1–2):157–79.
- [13] Ulusay R, Aydan O, Hamada M. The behavior of structures built on active fault zones: examples from the recent earthquakes in Turkey. In: *Seismic fault-induced failures—possible remedies for damage to urban facilities*. Japan: University of Tokyo; 2001. p. 1–26.
- [14] Russo M, Germani G, Amberg W. Design and construction of large tunnel through active faults: a recent application. In: *International conference of tunneling and underground space use*. Istanbul: Turkey; 2002. p. 16–18.
- [15] Johansson J, Konagai K. Fault induced permanent ground deformations: experimental verification of wet and dry soil, numerical findings' relation to field observations of tunnel damage and implications for design. *Soil Dyn Earthquake Eng* 2007;27:938–56.
- [16] Wang L. The characteristics of disasters induced by the Wenchuan  $M_w$  8.0 earthquake. In: Prakash S, editor. *China 2008, International conference on case histories in geotechnical engineering*. Washington, DC.
- [17] Lin A, Ren Z, Jia D, Wu X. Co-seismic thrusting rupture and slip distribution produced by the 2008  $M_w$  7.9 Wenchuan earthquake. *China Tectonophysics* 2009;471:203–15.
- [18] Paolucci R, Yilmaz MT. Simplified theoretical approaches to earthquake fault rupture—shallow foundation interaction. *Bull Earthquake Eng* 2008;6(4):629–44.
- [19] Gazetas G, Pecker A, Faccioli E, Paolucci R, Anastasopoulos I. Preliminary design recommendations for dip-slip fault—foundation interaction. *Bull Earthquake Eng* 2008;6(5):677–87.
- [20] Anastasopoulos I, Gerolymos N, Gazetas G, Bransby MF. Simplified approach for design of raft foundations against fault rupture. Part I: Free-field. *Earthquake Eng Eng Vib* 2008;7:147–63.
- [21] Anastasopoulos I, Gerolymos N, Gazetas G, Bransby MF. Simplified approach for design of raft foundations against fault rupture. Part II: Soil—structure interaction. *Earthquake Eng Eng Vib* 2008;7:165–79.
- [22] Loukidis D, Bouckovalas G. Numerical simulation of active fault rupture propagation through dry soil. In: Prakash S, editor. *Proceedings of the fourth international conference on recent advances in geotechnical earthquake engineering and soil dynamics*. CD-ROM, paper no. 3.04. San Diego, California University of Missouri-Rolla; 2001.
- [23] Lin ML, Chung CF, Jeng FS. Deformation of overburden soil induced by Thrust fault slip. *Eng Geol* 2006;88(1–2):70–89.
- [24] Anastasopoulos I, Gazetas G, Bransby MF, Davies MCR, El Nahas A. Fault rupture propagation through sand: finite element analysis and validation through centrifuge experiments. *J Geotech Geoenviron Eng ASCE* 2007;133(8):943–58.
- [25] Loukidis D, Bouckovalas G, Papadimitriou A. Analysis of fault rupture propagation through uniform soil cover. *Soil Dyn Earthquake Eng* 2009;29:1389–404.
- [26] Anastasopoulos I, Antonakos G, Gazetas G. Slab foundation subjected to thrust faulting in dry sand: parametric analysis and simplified design method. *Soil Dyn Earthquake Eng* 2010;30:912–24.
- [27] Baziar MH, Nabizadeh A, Jabbari M. Evaluation of fault—foundation interaction using numerical studies. In: *15th world conference on earthquake engineering*. Lisbon: Portugal; 2012.
- [28] Loli M, Bransby MF, Anastasopoulos I, Gazetas G. Interaction of caisson foundations with a seismically rupturing normal fault: centrifuge testing versus numerical simulation. *Geotechnique* 2012;62(1):29–43.
- [29] Ng CWW, Cai QP, Hu P. Centrifuge and numerical modeling of normal fault-rupture propagation in clay with and without a preexisting fracture. *J Geotech Geoenviron Eng ASCE* 2012;138(12):1492–502.
- [30] Chang YY, Lee CJ, Huang WC, Huang WJ, Lin ML, Hung WY, et al. Use of centrifuge experiments and discrete element analysis to model the reverse fault slip. *Int J Civil Eng* 2013;11(2):79–89.
- [31] Johansson J, Konagai K. Fault induced permanent ground deformations—simulations and experimental verification. In: *Proceedings 13th world conference on earthquake engineering \_DVD-ROM\_*, international association of earthquake engineering; 2004.
- [32] Johansson J, Konagai K. Fault induced permanent ground deformations an experimental comparison of wet and dry soil and implications for buried structures. *Soil Dyn Earthquake Eng* 2006;26(1):45–53.
- [33] Bransby F, Davies MCR, Elnahas A, Nagaoka S. Centrifuge modeling of normal fault—foundation interaction. *Bull Earthquake Eng Special Issue: Integrated approach to fault rupture— and soil—foundation interaction* 2008;6(4):585–605.
- [34] Bransby F, Davies MCR, Elnahas A, Nagaoka S. Centrifuge modeling of reverse fault—foundation interaction. *Bull Earthquake Eng, Special Issue: Integrated approach to fault rupture— and soil—foundation interaction* 2008;6(4):607–28.
- [35] Ahmed W, Bransby MF. Interaction of shallow foundations with reverse faults. *J Geotech Geoenviron Eng ASCE* 2009;135(7):914–24.
- [36] Moosavi SM, Jafari MK, Kamalian M, Shafiee A. Experimental investigation of reverse fault rupture—rigid shallow foundation interaction. *Int J Civil Eng* 2010;8(2):85–98.
- [37] Lin ML, Chung CF, Jeng FS, Yao TC. The deformation of overburden soil induced by thrust faulting and its impact on underground tunnels. *Eng Geol* 2007;92:110–32.
- [38] Lee CJ, Wang CR, Wei YC, Hung WY. Evolution of the shear wave velocity during shaking modeled in centrifuge shaking table tests. *Bull Earthquake Eng* 2011;10(2):401–20.
- [39] Lee CJ, Wu BR, Chen HT, Chiang KH. Tunnel stability and arching effects during tunneling in soft clayey soil. *Tunnelling Underground Space Technol* 2006;21:119–32.
- [40] Lee WJ, Hamada M. An experimental study on earthquake fault rupture propagation through a sandy soil deposit. *J Struct Eng Earthquake Eng JSCE* 2005;22:1–13.